Available online at www.sciencedirect.com
SCIENCE DIRECT®
ELSEVIER
International Journal of Solids and Structures 43 (2006) 2799–2819
INTERNATIONAL JOURNAL OF SOLIDS and STRUCTURES
www.elsevier.com/locate/ijsolstr

Application of a new constitutive model for the description of rubber-like materials under monotonic loading

Z. Guo *, L.J. Sluys

Faculty of Civil Engineering and Geosciences, Delft University of Technology, 2600GA Delft, The Netherlands

Received 27 January 2005; received in revised form 8 June 2005
Available online 16 August 2005

Abstract

The present paper is focused on the development of a constitutive model for the computational analysis of the mechanical behaviour of hyperelastic materials. One of the main obstacles in solving nonlinear elastic problems is the constitutive equation that must be as simple as possible but also realistic in the large strain range, especially for engineering purposes. Gao has proposed a relatively simple model that shows a good performance in tension as well as in compression. In this paper, the capabilities of Gao's model have been discussed. Three sets of experimental data of different types of deformation are used to identify the model parameters. Numerical simulations are in good agreement with experimental data. Comparisons with Ogden's formula and Mooney–Rivlin's formula by means of a theoretical and a numerical analysis demonstrate that Gao's model performs well for the description of hyperelastic material behaviour and covers a very large range of deformation. Another advantage of this model is that it only needs two parameters to predict the mechanical behaviour of hyperelastic materials. As an application, a singular problem of a wedge loaded by a concentrated tensile force is analysed.

Keywords: Rubber-like material; Constitutive modelling; Finite element method; Parameter estimation

1. Introduction

The variety of applications of rubber-like materials in different industrial areas is enormous. In the automotive industry, rubber is applied in tires, as engine seals and door seals, whereas in aerospace industry rubber rings are used in fuel systems. In other engineering fields, rubbers have been applied in conveyor belts, meteorological balloons and bearings of foundations. An increase of applications requires a better

* Corresponding author. Tel.: +31 15 278 5835; fax: +31 15 278 8162.
E-mail address: z.guo@citg.tudelft.nl (Z. Guo).

0020-7683/$ - see front matter
doi:10.1016/j.ijsolstr.2005.06.026

understanding of mechanical behaviour of rubber-like materials. Due to the complexity of rubber components, an important problem in nonlinear elasticity theory is to derive a reasonable and applicable elastic law, which is the key to the development of reliable analysis tools.

Many attempts have been made to develop a theoretical stress–strain relation that fits experimental results for hyperelastic materials (Charlton and Yang, 1994; Boyce and Arruda, 2000; Miehe et al., 2004). For example, Mooney (1940) proposed a phenomenological model with two parameters based on the assumption of a linear relation between the stress and strain during simple shear deformation. Later, Treloar (1958) published a model based on the statistical theory, the so-called neo-Hookean material model with only one material parameter. However, this was proved to be merely a special case of the Mooney model. The Mooney and neo-Hookean strain energy function have played an important role in the development of the nonlinear hyperelastic theory and its applications (Ogden, 1984, 2001). It has been proved by Bogert (1991) that the Mooney model performs well for moderately large deformation of uniaxial elongation and shear deformation. But, it cannot describe the S-curvature of the force–stretch relation in the uniaxial elongation experiment and the force–shear displacement relation in a shear experiment. In 1950, Rivlin (1948a,b, 1949) modified the Mooney model to obtain a general expression of the strain energy function expressed in terms of strain invariants. One of the successful models in this class has recently been developed by Yeoh (1993) in the form of a third-order polynomial of the first invariant of the right Cauchy–Green tensor. An alternative high-order polynomial model of the first invariant has been proposed by Gent (1996) and has the form of a natural logarithm.

In 1972, Ogden (1972a,b) proposed a strain energy function expressed in terms of principal stretches, which is a very general tool for describing hyperelastic material. An excellent agreement has been obtained between Ogden's formula and Treloar's experimental data for extensions of unfilled natural rubber up to 700% (Ogden, 1972a,b). However, the parameter identification is complicated because of the purely phenomenological character of the Ogden strain energy function.

Besides these purely phenomenological models, micro-mechanically based idealized network models have also been proposed. The first explicit expression for the configurational entropy of a single chain was given by Kuhn and Grun (1942). James and Guth (1941) proposed a model based on the assumption that the possible configurations of links in a chain are described by using a Gaussian distribution. This network model is frequently referred to as the three-Gaussian-chain model, which is available for small strains. For the large strain range, James and Guth (1943) and Wang and Guth (1952) proposed a non-Gaussian network model consisting of three independent sets of chains (each set contains $n/3$ chains per unit volume), a so-called three-chain model. Treloar (1946) and Flory and Rehner (1943) simplified the complex polymer network by a four-chain model, in which four non-Gaussian chains are connected to the corners of a tetrahedron. Later on, Arruda and Boyce (1993) developed an eight-chain model and Wu and van der Giessen (1993) proposed the so-called full-network model. Recently Boyce (1996) compared the eight-chain model to the first invariant-based Gent model and demonstrated the almost equivalence of these two models in the sense of their constructions and fitting qualities of test results. A more recent model, which is called the non-affine micro-sphere model has been proposed by Miehe et al. (2004).

Theoretical analysis and engineering application require the constitutive law to be expressed as simply as possible. However, simplicity often violates rationality. When we consider a problem with a singular point (such as a crack tip or a concentrated force), the situation is different from the finite deformation case (Knowles and Sternberg, 1973; Mooney, 1940). Actually, near a singular point in rubber-like materials, the strain goes to infinity, which complicates the problem. To reflect the material behaviour near a singular point, Gao proposed a simple elastic law that separately considers the resistance of materials to tension and compression (Gao, 1997). This constitutive relation was successfully used to analyse singular problems (Gao, 1997, 1999; Gao and Chen, 2001).

In this paper attention is restricted to the development of Gao's constitutive model (Gao, 1997) for computational analysis of the static behaviour of hyperelastic materials. In Section 2, Gao's constitutive elastic

law is presented as well as Drucker's stability postulate and parameters are discussed; Special subroutines are programmed to implement Gao's elastic law in the DIANA finite element package. Three sets of experiments under different loading conditions are described and estimations of material parameters of Gao's model are carried out in Section 3; numerical simulations are assessed on the basis of experimental data in this section. In Section 4, Gao's law is theoretically and numerically compared with Ogden's formula and Mooney–Rivlin's formula. In Section 5, a numerical analysis of a wedge loaded by a concentrated tensile force is compared to an analytical asymptotic solution.

2. Basic formula and elastic law

2.1. Basic formula

A three-dimensional domain of the material is considered. Before deformation, the base vectors along x^i direction at a point in curved coordinates are $\mathbf{e}_i$ $(i = 1, 2, 3)$ where $\|\mathbf{e}_i\| = 1$ and $\mathbf{e}_i \cdot \mathbf{e}_j = \delta_i^j$.

Let $\boldsymbol{\varepsilon} = \varepsilon_{ij}\mathbf{e}_i \otimes \mathbf{e}_j$ denote the Green strain tensor, and $\mathbf{U}$ be the unit tensor. The right Cauchy–Green strain tensor is obtained via

$$\mathbf{C} = 2\boldsymbol{\varepsilon} + \mathbf{U}, \tag{1}$$

in which

$$\mathbf{C} = g_{ij}\mathbf{e}_i \otimes \mathbf{e}_j, \tag{2}$$

with

$$g_{ij} = 2\varepsilon_{ij} + \delta_{ij}. \tag{3}$$

The strain invariants can be expressed as

$$I_1 = \mathbf{C} : \mathbf{U}, \qquad I_2 = \mathbf{C} : \mathbf{C}, \qquad I_3 = \mathbf{C}^2 : \mathbf{C}, \qquad I_{-1} = \mathbf{C}^{-1} : \mathbf{U}. \tag{4}$$

The following strain invariant is also used later:

$$I_2^* = \tfrac{1}{2}(I_1^2 - I_2). \tag{5}$$

For isotropic material, the strain energy per unit underformed volume W can be expressed by independent strain invariants. The second Piola–Kirchhoff stress reads

$$\boldsymbol{\tau} = \frac{\partial W}{\partial \boldsymbol{\varepsilon}} = \frac{\partial W}{\partial \mathbf{C}} \cdot \frac{\partial \mathbf{C}}{\partial \boldsymbol{\varepsilon}} = 2\frac{\partial W}{\partial \mathbf{C}}. \tag{6}$$

The incremental stress–strain relation is obtained by differentiation of the above equation one more time with respect to strain, so that

$$\frac{\partial \boldsymbol{\tau}}{\partial \boldsymbol{\varepsilon}} = \frac{\partial \boldsymbol{\tau}}{\partial \mathbf{C}} \cdot \frac{\partial \mathbf{C}}{\partial \boldsymbol{\varepsilon}} = 2\frac{\partial \boldsymbol{\tau}}{\partial \mathbf{C}} = 4\frac{\partial^2 W}{\partial \mathbf{C}^2}, \tag{7}$$

or in the form

$$\mathrm{d}\boldsymbol{\tau} = \mathbf{D}(\mathrm{d}\varepsilon_{11}, \mathrm{d}\varepsilon_{22}, \mathrm{d}\varepsilon_{33}, \mathrm{d}\varepsilon_{12}, \mathrm{d}\varepsilon_{23}, \mathrm{d}\varepsilon_{31})^{\mathrm{T}}, \tag{8}$$

where

$$\mathbf{D} = (D_{ij11}, D_{ij22}, D_{ij33}, D_{ij12} + D_{ij21}, D_{ij23} + D_{ij32}, D_{ij13} + D_{ij31}), \tag{9}$$

is the tangential stiffness matrix.

2.2. An elastic law

Gao proposed a strain energy function that separately considers the resistance of materials to tension and compression for hyperelastic and isotropic materials. Accordingly, a strain energy formulae that only contains two terms was given by Gao (1997):

$$W = a\left(I_1^n + I_{-1}^n\right), \tag{10}$$

where a and n are positive material parameters. In this model, no damping, energy loss, creep, relaxation or hysteresis are taken into consideration. The second Piola–Kirchhoff stress becomes

$$\boldsymbol{\tau} = 2\frac{\partial W}{\partial \mathbf{C}} = 2na\left(I_1^{n-1}\mathbf{U} - I_{-1}^{n-1}\mathbf{C}^{-2}\right). \tag{11}$$

The second Piola–Kirchhoff stress tensor is a useful stress measure for application in numerical programmes since it is calculated with respect to the known, undeformed configuration. For engineering purposes the Cauchy stress tensor is more appropriate. Both stress measures are related via

$$\boldsymbol{\sigma} = J^{-1}\mathbf{F}\cdot\boldsymbol{\tau}\cdot\mathbf{F}^{\mathrm{T}}, \tag{12}$$

where J is the Jacobian of the transformation. J represents the ratio of the actual volume of the infinitesimal body to the initial volume and can be calculated by the determinant of the deformation gradient

$$J = \sqrt{\det(\mathbf{C})} = \left[\tfrac{1}{6}\left(I_1^3 - 3I_1I_2 + 2I_3\right)\right]^{1/2}. \tag{13}$$

Let λ_i denote the values of principal strain, then

$$I_1 = \lambda_1^2 + \lambda_2^2 + \lambda_3^2, \qquad I_{-1} = \lambda_1^{-2} + \lambda_2^{-2} + \lambda_3^{-2}, \qquad J = \lambda_1\lambda_2\lambda_3. \tag{14}$$

The second Piola–Kirchhoff stress in Eq. (6) and the incremental stress–strain relation in Eq. (8) are basic equations for implementation of a hyperelastic material model in finite element software with the proposed strain energy function. So, substituting Eq. (10) into Eqs. (6) and (8), the second Piola–Kirchhoff stress and the incremental stress–strain relation can be derived.

Mooney–Rivlin, Ogden and Besseling (1983) models are available for hyperelastic behaviour in the finite element program DIANA. Special subroutines are programmed in order to implement Gao's elastic law in the DIANA software (Guo et al., 2003).

2.3. Discussion on Drucker's stability

It is important that the energy function obey the laws of thermodynamics when energy functions are used to relate stress and strain in finite element programs. In other word, energy functions should mathematically require the solid to increase its internal energy when we do work on it. Such energy functions are called stable. As pointed out by Johnson et al. (1994) that unstable energy functions can cause havoc in the nonlinear numerical solution algorithms used in finite element codes. Stability requires energy functions to obey a certain condition, which is known as Drucker's stability postulate that can be expressed as following:

$$\sum_i \mathrm{d}\sigma_i\,\mathrm{d}\varepsilon_i \geqslant 0, \tag{15}$$

where $\mathrm{d}\sigma_i$ is an increment in the ith principal Cauchy stress and $\mathrm{d}\varepsilon_i$ is an increment in the corresponding strain at any point in the solid. Therefore, the tangential stiffness matrix $\mathbf{D}$ should be positive definite. Johnson et al. derived Drucker's stability postulate for the form of Rivlin expansion under the condition of plane stress. A sufficient condition for the positive trace of $\mathbf{D}$ is that coefficients in Rivlin expansion

are nonnegative. To ensure the determinant of **D** to be positive, an additional requirement is needed (Johnson et al., 1994), namely

$$W_{11}W_{22} - W_{12}^2 > 0, \quad W_{ij} = \frac{\partial^2 W}{\partial I_i I_j}. \tag{16}$$

Because Gao's model is a polynomial function of invariants, the requirements of Drucker's stability postulate derived by Johnson et al. is also suitable for Gao's model. For incompressible material, I_{-1} is equal to I_2^*. Substituting Eq. (10) into Eq. (16), gives

$$\frac{\partial^2 W}{\partial I_1^2}\frac{\partial^2 W}{\partial I_{-1}^2} - \frac{\partial^2 W}{\partial I_1 \partial I_{-1}} = a^2 n^2 (n-1)^2 I_1^{n-2} I_{-1}^{n-2} - 0 > 0. \tag{17}$$

Generally, $a > 0$ and $1 > n > 3$ (Gao, 1997), so that Gao's model satisfies Drucker's stability postulate. Here, the power n is not necessarily an integer.

2.4. Numerical results and discussion on parameters

To demonstrate how material parameters of Gao's model influence the behaviour of rubber-like materials, we analyse a cube specimen loaded in uniaxial tension with Gao's constitutive law. We consider a cubic element with unit length. Under the action of normal stress working in x-direction, the edge lengths become λ, μ and μ, respectively, but the edges still remain perpendicular. By definition, we have

$$\mathbf{F} = \lambda \mathbf{e}_1 \otimes \mathbf{e}_1 + \mu(\mathbf{e}_2 \otimes \mathbf{e}_2 + \mathbf{e}_3 \otimes \mathbf{e}_3), \tag{18}$$

$$\mathbf{C} = \lambda^2 \mathbf{e}_1 \otimes \mathbf{e}_1 + \mu^2(\mathbf{e}_2 \otimes \mathbf{e}_2 + \mathbf{e}_3 \otimes \mathbf{e}_3), \tag{19}$$

$$\mathbf{C}^{-1} = \lambda^{-2} \mathbf{e}_1 \otimes \mathbf{e}_1 + \mu^{-2}(\mathbf{e}_2 \otimes \mathbf{e}_2 + \mathbf{e}_3 \otimes \mathbf{e}_3), \tag{20}$$

$$I_1 = \lambda^2 + 2\mu^2, \qquad I_{-1} = \lambda^{-2} + 2\mu^{-2}, \qquad J = \lambda\mu^2. \tag{21}$$

If we substitute Eqs. (18)–(21) and (11) into Eq. (12), the Cauchy stress becomes

$$\boldsymbol{\sigma} = \frac{2na}{\lambda\mu^2}\left(\left(I_1^{n-1}\lambda^2 - I_{-1}^{n-1}\lambda^{-2}\right)\mathbf{e}_1 \otimes \mathbf{e}_1 + \left(I_1^{n-1}\mu^2 - I_{-1}^{n-1}\mu^{-2}\right)(\mathbf{e}_2 \otimes \mathbf{e}_2 + \mathbf{e}_3 \otimes \mathbf{e}_3)\right). \tag{22}$$

For uniaxial tension, the conditions $\sigma_{yy} = \sigma_{zz} = 0$ give

$$(\lambda^2 + 2\mu^2)^{n-1}\mu^2 - (\lambda^{-2} + 2\mu^{-2})^{n-1}\mu^{-2} = 0. \tag{23}$$

Then Eq. (22) becomes

$$\boldsymbol{\sigma} = \frac{2na}{\lambda\mu^2} I_1^{n-1}\left(\lambda^2 - \frac{\mu^4}{\lambda^2}\right)\mathbf{e}_1 \otimes \mathbf{e}_1. \tag{24}$$

When $\lambda \gg 1$ ($\mu \ll 1$), Eq. (23) gives

$$\mu = \left(\frac{\sqrt{2}}{\lambda}\right)^{\frac{n-1}{n+1}}. \tag{25}$$

Eqs. (24) and (25) can be combined to give

$$\boldsymbol{\sigma} = 2^{\frac{2}{n+1}} na \lambda^{2n+1-\frac{4}{n+1}} \mathbf{e}_1 \otimes \mathbf{e}_1. \tag{26}$$

The total load is

$$L = \mu^2 \sigma = 2na\lambda^{2n-1}. \tag{27}$$

This equation shows that parameter a is directly proportional to the stiffness of the rubber material and parameter n not only influences the stiffness of the rubber material but also the curvature of the load–displacement diagram.

The numerical results are shown in Fig. 1(a) where we fix parameter $n = 2$, and take $a = 0.1, 0.5, 1.0, 2.0, 10.0$. In this picture, the solid lines are the results from numerical calculations and the circles are the theoretical results from Eq. (27). It is shown that our numerical results are in good agreement with the theoretical results, especially, for large deformations. But, relatively small differences at small deformation exist because the theoretical results from Eq. (27) are achieved under the condition of large deformations. Fig. 1(b) shows the loading force varying with material parameter a at uniaxial displacement $\lambda = 2$.

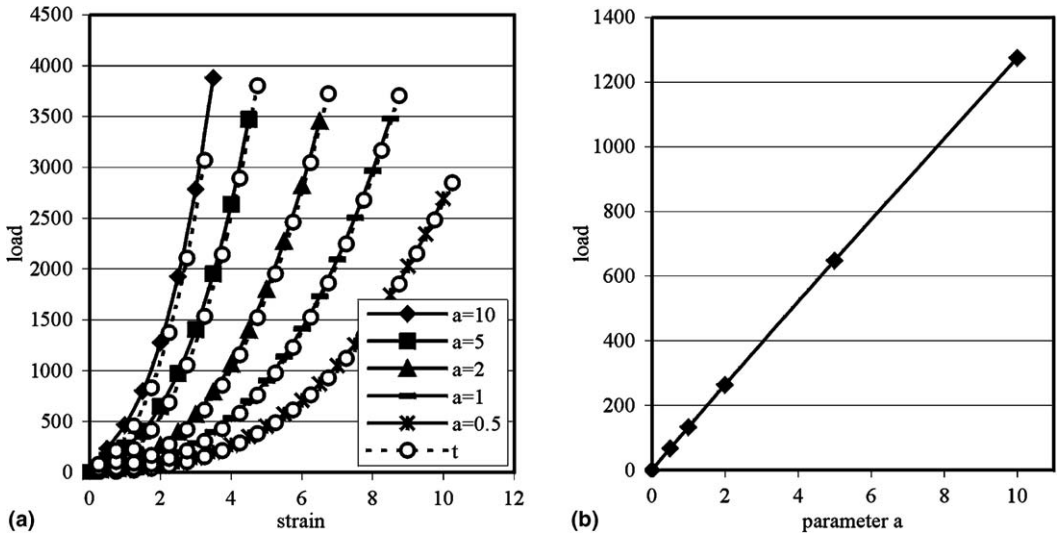

Fig. 1. Load–displacement curves: (a) for different a ($n = 2$) and (b) at displacement $\lambda = 2$ ($n = 2$).

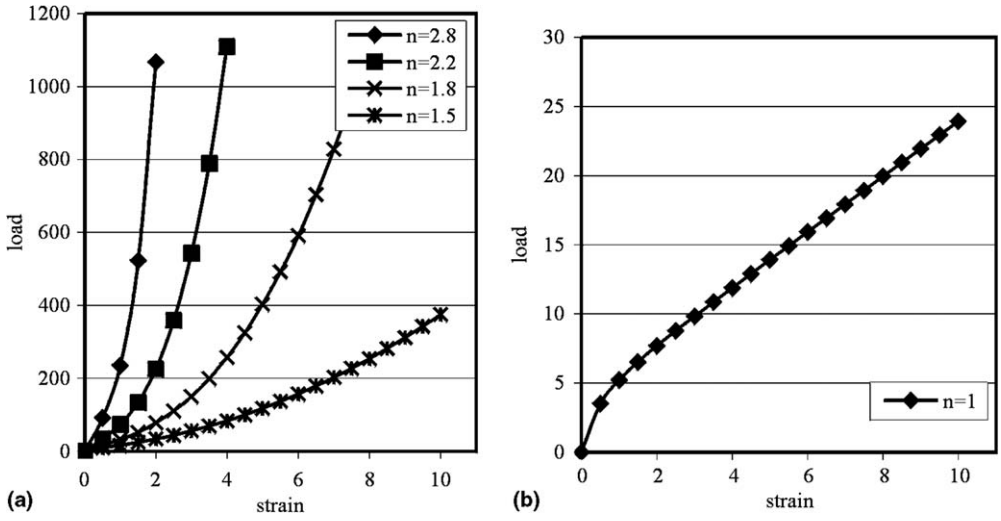

Fig. 2. Load–displacement curves: (a) for different $n > 1.5$ ($a = 1$) and (b) for $n = 1$ ($a = 1$).

It illustrates that the stiffness is linearly increasing with parameter a. This conclusion is similar to a result obtained from theoretical analysis.

Fig. 2 illustrates the numerical calculations, in which we plot the load versus the displacement by variation of material parameter n from 1 to 2.8 and fixing parameter $a = 1$. It is clearly shown that the stiffness and the curvature of the load–displacement diagram change when a different value for parameter n is used.

The load–displacement curves in Figs. 1 and 2 indicate that different nonlinear rubber-like materials can be simulated by the constitutive law of Eq. (10) by means of properly selecting the material parameters a and n. Further verification will be done in the next section.

3. Estimation of material parameters and numerical simulation

3.1. Experimental results

The verification of the numerical modelling cannot be restricted only to the simple tension case, because the aim of numerical modelling of rubber-like material should be that a model is capable of predicting the mechanical behaviour of any type of strain. To fulfil this goal, we examine certain simple types of deformation to evaluate if the elastic law possesses the significant features of hyperelastic materials.

In this section, three sets of experimental results are used to assess the constitutive model. Firstly, an experimental result is taken from Mullins and Tobin (1957) for a simple tension test. Secondly, simple tension and compression tests were carried out in the Institute of Thermomechnics (Pozivilova, 2003). The third experiment was carried out at the French Research Department (Chagnon et al., 2004) for the combined deformation of tension and pure shear.

3.1.1. Simple tension test

Many different tension tests on rubber specimens were carried out in the past. We have chosen the experimental result of Mullins and Tobin (1957) for a simple tension test because this experiment was done under cyclic loading and the data can also be used for a damage modelling of the material in a forthcoming paper.

The material used for the tension test was made of synthetic GR-S (government rubber-styrene) tire tread vulcanizate containing MPC black. The stress–strain measurements were carried out at 25 °C on parallel-sided rubber strips, which are about 3 mm wide and 1 mm thick. The initial marked length was 1 in. (25.4 mm). Light clamps were attached to the ends of the specimen, which was supported from the upper one while stresses were applied by hanging weights at the lower end. The displacement between reference marks was measured three minutes after each increment of load in order to minimize the creep effect (Mullins and Tobin, 1957). A typical stress–strain diagram of the loading path is shown in Fig. 3. The strains and stresses were calculated relative to the original dimensions of the test specimen.

3.1.2. Simple tension and compression test

The specimen used for a tension and compression test (Pozivilova, 2003) was a cylinder from soft rubber with a diameter of 11.5 mm. The initial marked length for tension was 200 mm. The loading of the specimen was supposed to be slow enough to reduce the visco-elastic effect of the rubber material and its hysteresis behaviour. Because the length of the elongated specimen was much higher than the measured length, the one-dimensional stress state was achieved during the tension test with sufficient accuracy.

The original length for compression was 10.15 mm. It was much shorter than the specimen in the tension test in order to avoid buckling of the specimen. The specimen was compressed to less than half of its original length. The stress field of the specimen is not uniaxial during compression. Even if the heads of the testing machine were greased, they still prevented extension of the diameter of the cylindrical specimen on the pressure heads.

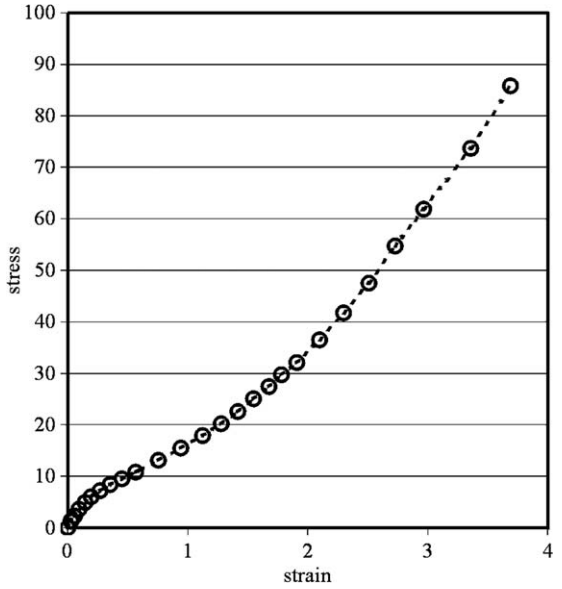

Fig. 3. Stress–strain curve on GR-S tread vulcanizate.

The measured load–stretch curve is given in Fig. 4 for both tension and compression. The tension data are in the right side of the graph with stretch larger than 1. The breaking of the rubber specimen occurred for an elongation of approximately 200%. The compression data are in the left side of the diagram with a stretch less than 1.

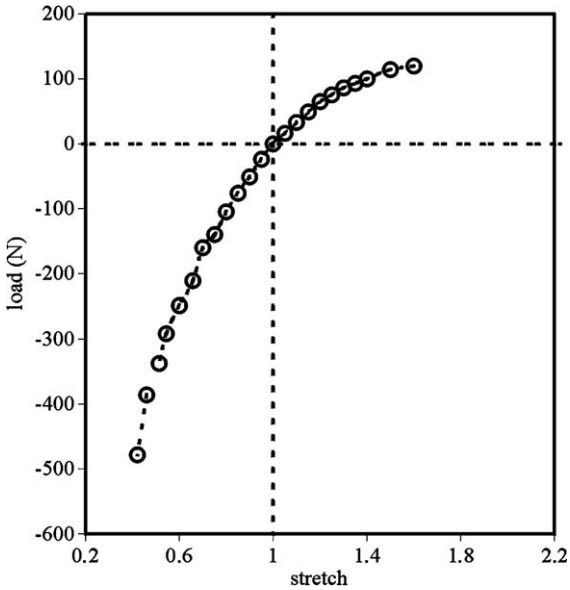

Fig. 4. Load–stretch curve obtained from tension and compression tests.

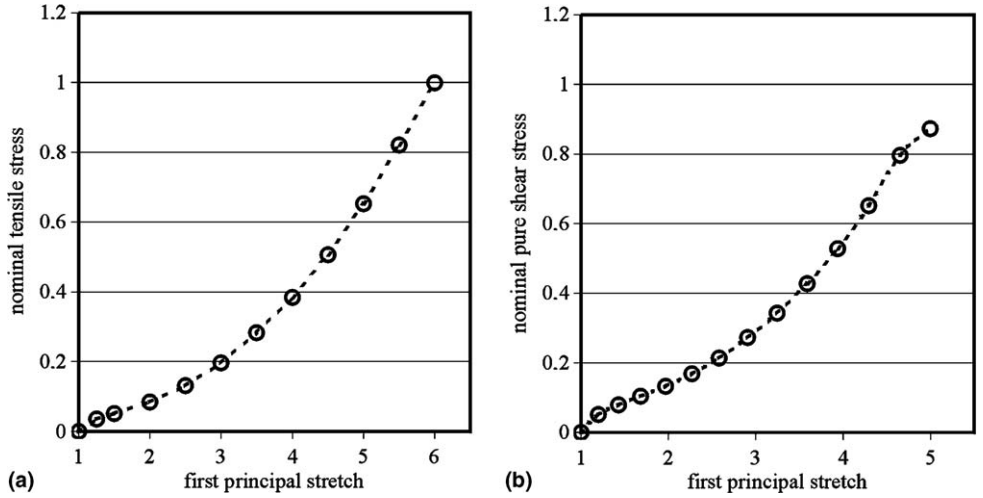

Fig. 5. Experimental data of stress–stretch curves: (a) simple tensile and (b) pure shear.

3.1.3. Simple tension and pure shear tests

Another experimental test for verification purposes was a tension and shear experiment, which was conducted in the French Research Department by Chagnon et al. (2004). The material used for this experiment is a carbon black filled natural rubber. The percentage of fillers is about 30%. The uniaxial tensile tests were conducted on flat coupon specimens and the simple shear specimens are blocks. All experiments were performed under displacement control.

The simple shear experimental data are transformed into pure shear data in order to simplify the analysis, because the analysis of simple shear experiments leads to difficulties for determination of material parameters due to an indefinite principal direction of the strain. This transformation of the experimental data from simple shear to pure shear is based on a proposal of Charlton and Yang (1994). Fig. 5(a) shows the nominal tensile stress against the first principal stretch curve under uniaxial tension. Fig. 5(b) is a result for pure shear data, in which the stresses are normalized by the maximum tensile stress.

3.2. Estimation of material parameters

The DIANA finite element package provides a parameter estimation module, which is based on a weighted least squares approach. The main idea is based on a comparison between experimental data and the outcome of the finite element model, followed by the determination of updated estimations of the material parameters.

It is assumed that the observational data from experiments consist of a set of vectors with data $\mathbf{y}_k$, $k = 1, \ldots, N$, where k indicates a load set or a discrete time parameter. Each vector contains values of measurable properties, such as displacements or forces. The observational data are considered to be a nonlinear function of a set of unknown material parameters $\mathbf{x}$:

$$\mathbf{y}_k = \mathbf{h}_k(\mathbf{x}) + \mathbf{v}_k. \tag{28}$$

Function $\mathbf{h}_k$ is the result of the finite element model and represents the dependence of the kth observation on $\mathbf{x}$ if there were no observation errors. These errors are presented by a vector $\mathbf{v}_k$.

First, only one vector of observational data $\mathbf{y}_1$ is considered to estimate parameter vector $\mathbf{x}$. The estimator can be specified from the model, an uncertainty model for $\mathbf{v}_1$ and a priori knowledge of $\mathbf{x}$. The optimal parameter vector $\mathbf{x}$ based on $\mathbf{y}_1$ is obtained by minimizing the following quadratic expression:

$$S_1 = (\mathbf{y}_1 - \mathbf{h}_1(\mathbf{x}))^{\mathrm{T}}\mathbf{R}_1^{-1}(\mathbf{y}_1 - \mathbf{h}_1(\mathbf{x})) + (\hat{\mathbf{x}}_0 - \mathbf{x})^{\mathrm{T}}\mathbf{Q}_1^{-1}(\hat{\mathbf{x}}_0 - \mathbf{x}), \tag{29}$$

where $\mathbf{x}_0$ is an initial guess for the parameter vector $\mathbf{x}$. Matrix $\mathbf{R}_1$ is a nonnegative symmetric matrix, which represents the covariance matrix of the residuals $\mathbf{v}_1$ and $\mathbf{Q}_1$ is a positive symmetric matrix, which represents the covariance matrix of the estimation error in $\mathbf{x}_0$. The introduction of $\mathbf{Q}_1$ makes it possible to adjust weight to a priori estimate $\mathbf{x}_0$ and less weight to the displacements $\mathbf{y}_1$. In many applications it is common to know the mean and variance of the expected residuals. In general, it can be stated that the larger $\mathbf{Q}_1$, the smaller the influence of $\mathbf{x}_0$.

To minimize the misfit function of Eq. (29), more methods were proposed. A traditional way is to use the Newton method (Tarantola, 1987)

$$\mathbf{x}^{(i+1)} = \mathbf{x}^{(i)} - \left(\frac{\partial^2 S}{\partial \mathbf{x}^2}\right)^{-1}_{\mathbf{x}^{(i)}} \left(\frac{\partial S}{\partial \mathbf{x}}\right)_{\mathbf{x}^{(i)}}, \tag{30}$$

in which

$$\left(\frac{\partial S}{\partial \mathbf{x}}\right)_{\mathbf{x}^{(i)}} = \left(\mathbf{H}^{(i)^{\mathrm{T}}}\mathbf{R}^{-1}\left(\mathbf{h}(\mathbf{x}^{(i)}) - \mathbf{y}\right) + \mathbf{Q}^{-1}\left(\mathbf{x}^{(i)} - \mathbf{x}^{(0)}\right)\right), \tag{31}$$

$$\left(\frac{\partial^2 S}{\partial \mathbf{x}^2}\right)_{\mathbf{x}^{(i)}} \approx \left(\mathbf{H}^{(i)^{\mathrm{T}}}\mathbf{R}^{-1}\mathbf{H}^{(i)} + \mathbf{Q}^{-1}\right). \tag{32}$$

Using Eqs. (30)–(32), we arrive at the following algorithm:

$$\mathbf{x}^{(i+1)} = \mathbf{x}^{(i)} + \left(\mathbf{H}^{(i)^{\mathrm{T}}}\mathbf{R}^{-1}\mathbf{H}^{(i)} + \mathbf{Q}^{-1}\right)^{-1} \times \left(\mathbf{H}^{(i)^{\mathrm{T}}}\mathbf{R}^{-1}\left(\mathbf{y} - \mathbf{h}(\mathbf{x}^{(i)})\right) + \mathbf{Q}^{-1}(\mathbf{x}^{(0)} - \mathbf{x}^{(i)})\right), \tag{33}$$

where the superscripts refer to the iteration number and where the subscripts are temporarily dropped. In each iteration, the procedure executes $m + 1$ complete finite element calculations, where m is the number of parameters. The m calculations are carried out to determine a matrix $\mathbf{H}_1^{(i)}$ numerically, as a linearization of $\mathbf{h}_1$ with respect to the most recent estimation $\mathbf{x}_1^{(i-1)}$.

The sequential property of the estimator from Eq. (33) is clear when a vector $\mathbf{y}_2$ with additional observational data from experiment is available. This can be data from another load set or from another point in time. These data can be used together with the initial conditions $\mathbf{x}_1$, $\mathbf{R}_2$ and $\mathbf{Q}_2$ resulting in an improved estimation $\mathbf{x}_2$.

To determine the material parameters several sets of experimental data for each experimental loading condition are considered as target values of material points. Since material parameter n varies from 1–3, we assume n to be a certain value and then estimate material parameter a. Fig. 6 shows the curves of parameter a obtained via the inverse technique. The experimental data are indicated by different symbols on the curves and observed at different displacements in the tensile test. For $n = 1.75$ the value of a converges rapidly to a constant value.

3.3. Results

3.3.1. Simple tension test

Since the experimental results are obtained under uniaxial tensile stress, it is easy to build up the finite element model. We can use one solid element to represent the cubic specimen. The value of the total computational tensile force is equal to the value of stress for Mullins and Tobin simple tension test if one solid

element with unit length is used, because the stress in the experiment is calculated based on the undeformed dimensions of the test specimen.

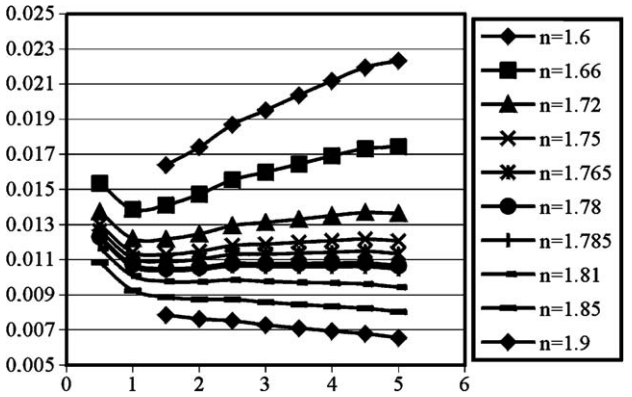

Fig. 6. The inverse identification of parameter a against iteration number (represented by different strain levels) for different n.

Table 1
Estimated values of material parameters

Experiment	Material parameters	Values
Simple tension test	a	0.75
	n	1.62

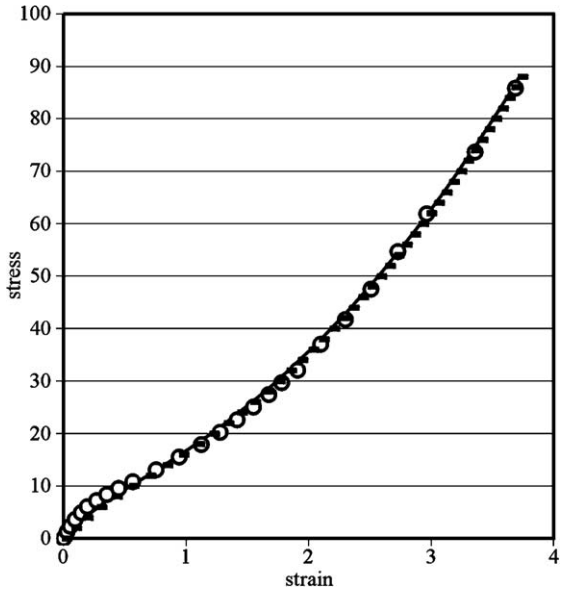

Fig. 7. Comparison of numerical results and experimental data for the Mullins and Tobin test: (○) experimental data and (■) numerical result.

The values of the material parameters estimated from the simple tension test, according to the procedure described in the Section 3.2, are presented in Table 1. Fig. 7 shows that computational results are in good agreement with the experiments for the simple tension test.

3.3.2. Simple tension and compression test

The material parameters estimated for tension and compression test are based on tension test data (see Fig. 4). The results are listed in Table 2. In order to compare the experimental data and numerical results for a simple tension test, the load calculated on a unit cubic solid element is multiplied by the ratio of area of cross-section of the experimental specimen to the area of a cross-section of the unit cube due to the uniaxial stress state. The result is shown in Fig. 9 (stretch larger than 1).

Because the requirement of a uniaxial stress condition in a compression test is not satisfied, the material parameters derived from the tension test data have to be checked in the compression regime.

The cylindrical specimen for compression is axisymmetric and symmetric to the plane dividing the cylinder into two equal parts. So, an axisymmetric analysis of a half cylinder was used in the finite element calculation. The finite element model is given in Fig. 8. The FEM model is built up from eight-node axisymmetric elements with one pressure node. The pressure head of the testing machine is modelled by one axisymmetric element with a stiffness, which is five orders higher than the stiffness of the specimen. The model consists of 626 elements and includes 1983 nodes. Adequate boundary conditions were prescribed to agree with the experimental conditions.

(1) All nodes in the axis of symmetry of the specimen and the pressure head only can move within the initial axis of symmetry.
(2) The displacements of the nodes of the specimen at the horizontal contact surface were prevented from moving in the radial direction, because of high friction between the specimen and pressure head of the testing machine.

Table 2
Estimated values of material parameters

Experiment	Material parameters	Values
Tension and compression	a	0.2625
	n	1.05

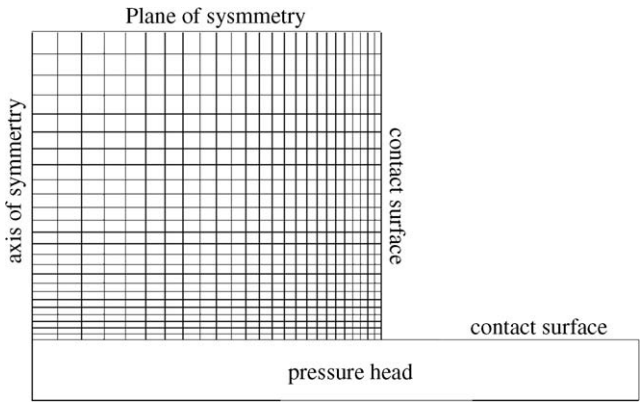

Fig. 8. FEM model of a quarter of the cross-section of the cylindrical specimen.

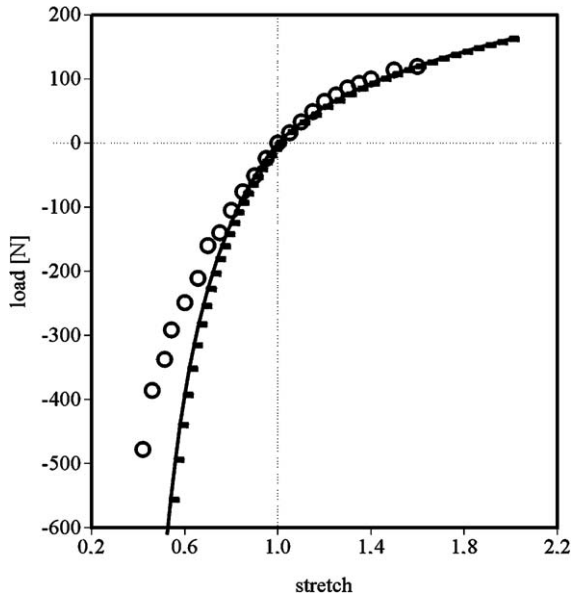

Fig. 9. Comparison of numerical results and experimental data for the simple tension and compression tests: (○) experimental data and (■) numerical results.

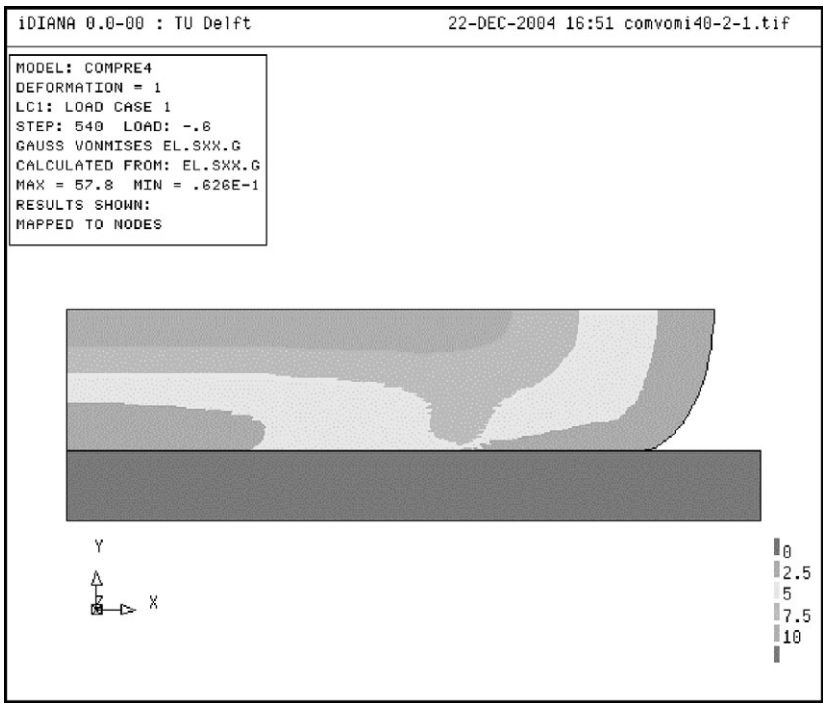

Fig. 10. The stress distribution on the deformed mesh for compression of the cylinder simulated by Gao's formulation.

(3) The contact boundary conditions between the pressure head and the bottom of the specimen were prescribed. The specimen and pressure head are connected by sharing one node on the axis of symmetry because of the continuity of displacement.
(4) To avoid the rolling of the rubber over the edge of the cylinder, the contact boundary conditions between the pressure head and the wall of specimen were also prescribed.

An identical displacement was prescribed at all nodes in the upper cross-section of the cylinder. The loading force can be calculated as a sum of reactions in all nodes belonging to the bottom of the pressure head.

Fig. 9 illustrates the comparison between the experimental data and numerical results. We can see that Gao's model is very suitable for describing the mechanical response in both the tension regime of the loading (stretch larger than 1) and the compression regime (stretch smaller than 1).

The distribution of the Von Mises stress on the deformed specimen for compression to 40% of its original length is given in Fig. 10. After a certain amount of deformation is reached (approximately to 80% of the original length), the contact boundary conditions between the lateral surfaces of the cylindrical specimen and pressure head were activated.

3.3.3. Simple tension and pure shear tests

The experimental data of both tension and pure shear are used to estimate the material parameters. Table 3 gives the values of the material parameters. The numerical results for tension and pure shear

Table 3
Estimated values of material parameters

Experiment	Material parameters	Values
Tension and pure shear	a	0.012
	n	1.75

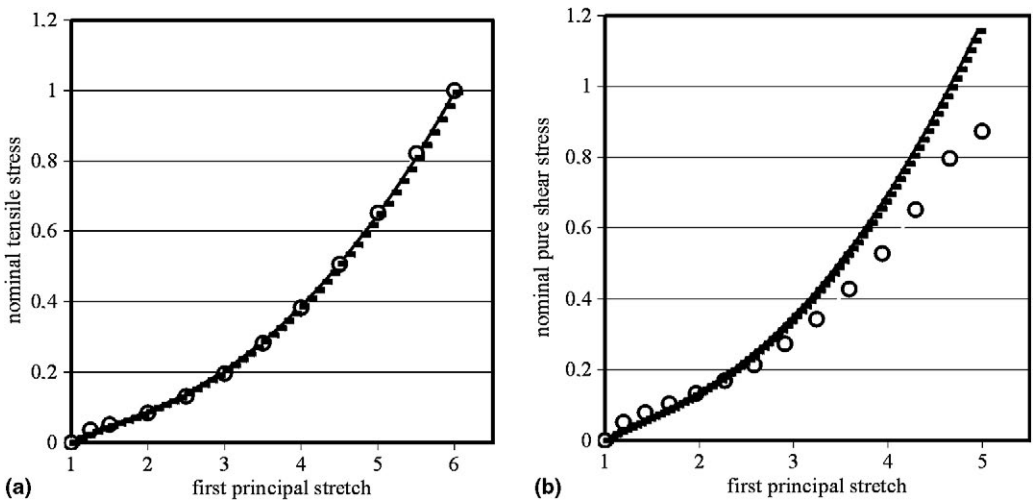

Fig. 11. Comparison of numerical results and experimental data for Chagnon etc. test, (a) uniaxial tensile test (b) pure shear test: (○) experimental data and (■) numerical result.

were compared with experimental data in Fig. 11, respectively. Fig. 11(a), similar to the results in Figs. 7 and 9, gave more evidence to support the statement that the computational results were in good agreement with the experiments for the simple tension test.

Fig. 11(b) indicates that the correspondence between the computational results and experimental data for the pure shear deformation is relatively good up to a certain amount of strain (over 300%). Beyond this strain level, the experimental and computational curves start to deviate somewhat. One reason could be that this model is based on the concept that the material should have resistance to tension and compression.

It is important to emphasize that in our examples the same material parameters are valid for different loading modes applied to the specimens from the same material. This property is crucial for the general use of Gao's elastic law.

4. Relation of Gao's model with other strain energy functions

4.1. Comparison of formulae

Ogden's model and Mooney–Rivlin's model are commonly used by many researchers. Relations between the Gao's model and the Ogden's model and the Mooney–Rivlin's model can be derived. Ogden (1972a,b) proposed a general but convenient form of the strain energy function, which can be written as

$$W = \sum_{i}^{n_i} \mu_i \phi(\alpha_i) + F(K), \tag{34}$$

where μ_i are constants, K is an invariant related to the relevant volume ratio

$$K = \tfrac{1}{6}\left(I_1^3 - 3I_1 I_2 + 2I_3\right) = \lambda_1^2 \lambda_2^2 \lambda_3^2 = J^2, \tag{35}$$

in which λ_i are the principal stretches and $\phi(\alpha_i)$ are strain invariants with exponent α_i that may not be integers,

$$\phi(\alpha_i) = \left(\lambda_1^{\alpha_i} + \lambda_2^{\alpha_i} + \lambda_3^{\alpha_i} - 3\right)/\alpha_i. \tag{36}$$

If $F \equiv 0$ and only two terms are taken into account in Ogden's model, Eq. (34) gives

$$W = \frac{\mu_1}{\alpha_1}\left(\lambda_1^{\alpha_1} + \lambda_2^{\alpha_1} + \lambda_3^{\alpha_1} - 3\right) + \frac{\mu_2}{\alpha_2}\left(\lambda_1^{\alpha_2} + \lambda_2^{\alpha_2} + \lambda_3^{\alpha_2} - 3\right). \tag{37}$$

If we choose

$$n_i = \alpha_1 = 2, \qquad \alpha_2 = -2, \qquad \mu_1 = 2a, \qquad \mu_2 = -2a. \tag{38}$$

Ogden's model becomes equivalent to Gao's model, for the case of $n = 1$ Ogden obtained a sufficient condition for satisfying Hill's constitutive inequality,

$$\mu_i \alpha_i > 0 \quad (\text{each } i \text{ no summation}). \tag{39}$$

Evidently, Gao's model satisfies this condition for $n = 1$. As for the general case, $1 < n < 3$, Gao's model is not equivalent to Ogden's model. For that case, Hill's inequality is difficult to proof, but the analysis and discussion on Drucker's stability postulate directly revealed reasonable values of n.

Another strain energy function was introduced by Mooney–Rivlin

$$W = C_1(I_1 - 3) + C_2(I_2^* - 3), \tag{40}$$

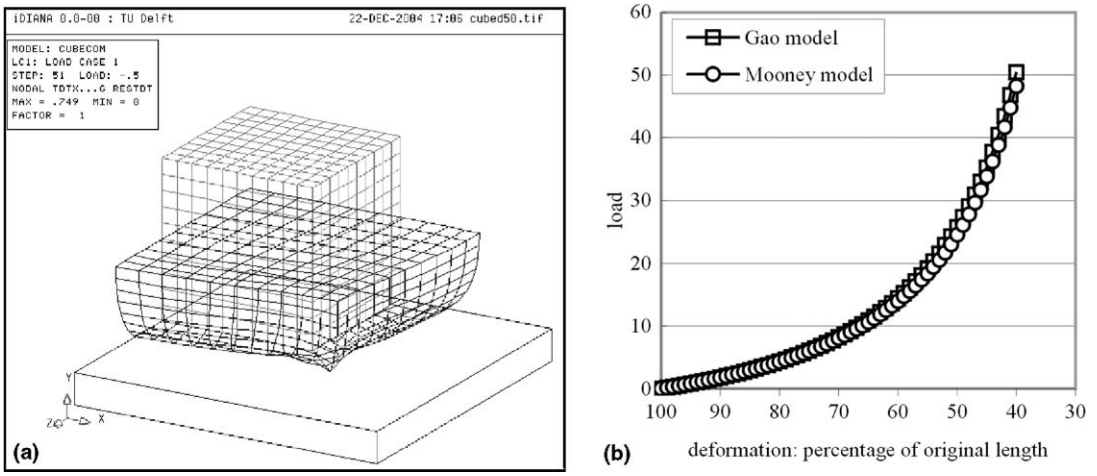

Fig. 12. (a) Deformed FEM model of one eighth of cube, (b) load–displacement curves with Gao's model and Mooney–Rivlin's model under confined compression, $n = 1$ and $a = C_1 = C_2 = 1$.

with C_1 and C_2 as the material parameters. When $n = 1$ and $a = C_1 = C_2 = 1$, the Mooney–Rivlin's strain energy function is equivalent to Gao's model.

Fig. 12 is the numerical comparison between Gao's and Mooney's models by using a cube under confined compression, in which all nodes in upper and bottom surfaces of the cube were prevented from moving within the surface. Because of symmetry only one eighth of the specimen is considered in the FEM calculation. Compression was prescribed in all nodes of the upper symmetric surface. Similar to the analysis of axisymmetric compression in Section 3.3.2, a contact boundary condition is used between the bottom surface of rubber and the support element as well as between the wall of rubber and the support element in order to easily pick up the reaction force and avoid the rolling of the rubber over the edge of the cube. Fig. 12(a) shows the deformed cube. Fig. 12(b) illustrates the equivalent numerical results of the two models.

In this numerical calculation, FEM meshes with different fineness are used to demonstrate convergence of the result. In this example, when the number of elements is larger than $5 \times 5 \times 5$ the reaction force remains constant.

4.2. Numerical simulations using different material models

Mechanical behaviour of rubber-like materials can be described with Ogden's model. The Mullins and Tobin experimental data was also analysed with this model (Ogden and Roxburgh, 1999). The correspondence between the Ogden model and experimental data was good, however six material parameters were needed in this fitting result. This is not convenient for practical application. It may be difficult to obtain all parameters since the database of experimental results is limited.

We use the same experimental data to estimate the material parameters of the Mooney–Rivlin model and obtain the material parameters $C_1 = 7.5$, $C_2 = -2.9$. The identification results are compared with Mullins and Tobin experimental data in Fig. 13(a). It is clearly shown that the Mooney–Rivlin results are in good agreement with the experimental results up to a certain level of deformation and the identification process is relatively simple since only two parameters have to be determined.

Fig. 13(b) presents the identification results of Gao's model compared with Mullins and Tobin experimental data. The material parameters are listed in Table 1. Almost no difference between numerical results

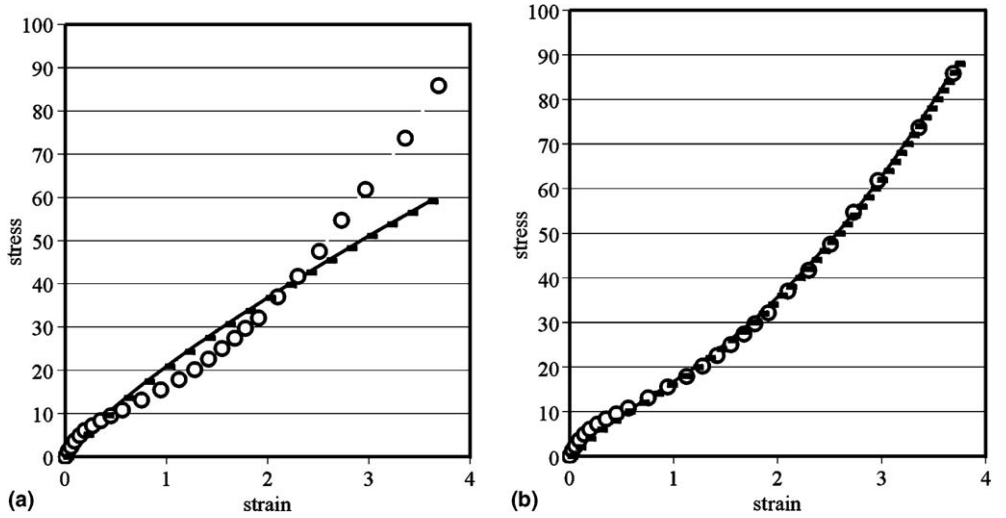

Fig. 13. Comparison of simulation results and experimental data for Mullins and Tobin test: (a) Mooney–Rivlin model and (b) Gao model: (○) experimental data and (■) numerical result.

and experimental data exists, also for the larger deformation range. The Gao model, similar to the Mooney–Rivlin model, only needs the estimation of two material parameters.

Based on analyses and comparisons in Sections 3 and 4, we can conclude that Gao's elastic law possesses fundamental characteristics and advantages in predicting the mechanical behaviour of rubber-like materials.

5. Analysis of wedge loaded by a concentrated tensile force

5.1. Asymptotic analyses

A schematic sketch of a wedge before and after deformation is shown in Fig. 14, respectively. Two Lagrangian coordinates are taken such that (R, Θ, Z) are the polar coordinates before deformation while (r, θ, z) are the polar coordinates after deformation. In this paper we consider a plane strain case, i.e., $Z = z$. We assume that the deformation near the tip can be described by the following mapping functions:

$$\begin{cases} R = r^{1+\beta} f(\zeta), \\ \Theta = g(\zeta), \quad \zeta = \theta r^{-\alpha}, \ \ 0 \leqslant \zeta \leqslant \zeta_0, \end{cases} \tag{41}$$

where α and β are positive constants to be determined, f and g are unknown functions and ζ_0 is the value of ζ on the free boundary.

If we substitute Eqs. (41) and (4) into Eq. (12) we obtain the Cauchy stress expression. In order to simplify the expression we introduce a new coordinate system (η, ζ) in the vicinity of $\theta = 0$, which yields

$$\eta = r\left(1 + \frac{\alpha}{2}\theta^2 + \frac{\alpha^2}{8}\theta^4 + \frac{\alpha^3}{48}\theta^6 + \cdots\right). \tag{42}$$

The inverse expression of Eqs. (42) and (41) can be written as

$$\begin{cases} r = \eta\left(1 - \frac{\alpha}{2}(\zeta\eta^{\alpha})^2\right), \\ \theta = \zeta\eta^{\alpha}. \end{cases} \tag{43}$$

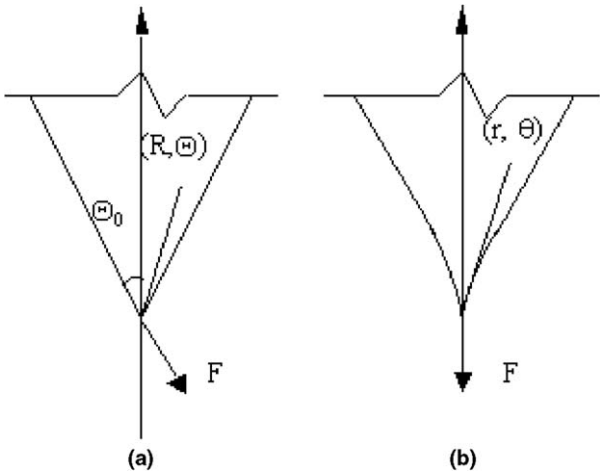

Fig. 14. Polar coordinates: (a) before deformation and (b) after deformation.

According to Eq. (43) and neglecting the higher-order terms, we can obtain the Cauchy stress in the (η,ζ) coordinate system

$$\boldsymbol{\sigma} = 2na\eta^{-\lambda}\left(T\mathbf{e}_\eta \otimes \mathbf{e}_\eta + \eta^{2\alpha}W\mathbf{e}_\zeta \otimes \mathbf{e}_\zeta + \eta^{\alpha}S(\mathbf{e}_\eta \otimes \mathbf{e}_\zeta + \mathbf{e}_\zeta \otimes \mathbf{e}_\eta)\right) \tag{44}$$

in which

$$\begin{aligned} &\lambda = (1+\alpha),\\ &\begin{cases} T = v^{1-2n}u^n,\\ w = v(v^{-2n}u^{n-1}(1+\beta)^2f'^2 - u^n),\\ S = -v^{1-2n}u^{n-1}(1+\beta)ff', \end{cases} \end{aligned} \tag{45}$$

where

$$\begin{cases} v = (1+\beta)f^2g',\\ u = f'^2 + f^2g'^2,\\ \beta = \dfrac{1}{2(n-1)}, \qquad \alpha = \dfrac{n}{n^2-1}. \end{cases} \tag{46}$$

Considering Eqs. (44)–(46) and the equilibrium condition as well as neglecting the higher-order terms, gives

$$\begin{cases} \dfrac{\mathrm{d}S}{\mathrm{d}\zeta} + \dfrac{S}{\zeta} = 0,\\ \dfrac{\mathrm{d}w}{\mathrm{d}\zeta} + \dfrac{w}{\zeta} + \alpha(1+\alpha)\zeta T + (1+2\alpha)S = 0. \end{cases} \tag{47}$$

The boundary conditions are

$$\begin{cases} g(0) = 0,\\ g'^4B^{n-1} = (1+\beta)^{2-2n}f_0^{-4n} \quad \text{when } g = \Theta_0, \end{cases} \tag{48}$$

$$S \equiv 0, \tag{49}$$

$$f = f_0 = \text{constant}. \tag{50}$$

Eq. (48) contains two boundary conditions for the second equation in Eq. (47) so that g can be solved numerically. We determine f_0 by considering the balance condition of load F with the resultant force of the field. By integration we have

$$F = \int (\sigma^{rr}\cos\theta - \sigma^{r\theta}\sin\theta) r \,\mathrm{d}\theta = \int \sigma^{rr} r \,\mathrm{d}\theta = 4n\alpha\Theta(1+\beta)^{-2n} f_0^{1-2n} \tag{51}$$

or

$$f_0 = \left(\frac{F}{4na\Theta_0}\right)^{-\beta} (1+\beta)^{-1-\beta}. \tag{52}$$

We obtain an asymptotic solution of stress state near the tip of the wedge.

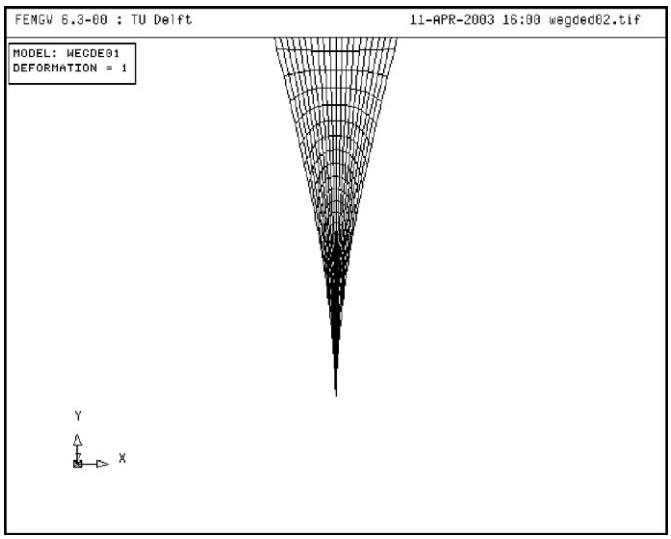

Fig. 15. Deformation of a wedge vertically loaded by a concentrated tensile force.

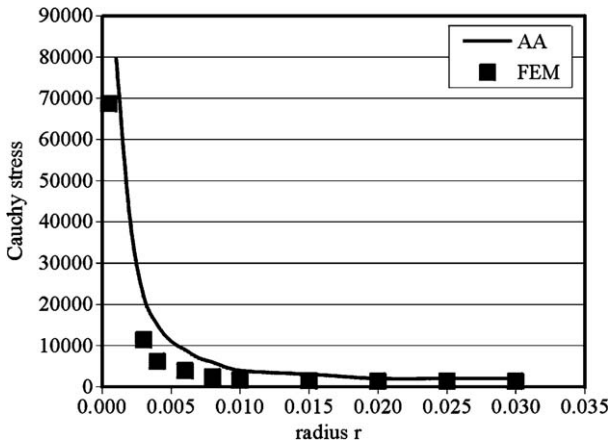

Fig. 16. Comparison of calculated and theoretical curves of Cauchy stress σ^{rr} versus radius r.

5.2. Finite element calculation

Because the asymptotic solution of the stress state is only available near the tip of the wedge, the numerical specimen (as shown in Fig. 14(a)) has a geometry with $\Theta_0 = \pi/6$ and $R_{\max} = 1.0$ when $\Theta_0 = 0$. The numerical calculation is carried out under a plane strain condition. The material parameters are taken as $a = 10$, $n = 2$ and the load $F = 0.5$ N. The shape of the wedge near the tip after deformation is shown in Fig. 15. The calculated curve of Cauchy stress σ^{rr} versus radius r (denoted as curve FEM) and the theoretical curve from Eq. (44) (denoted as curve AA) for $\Theta = 0$ are plotted in Fig. 16. It is shown that when r is small enough, the numerical results are consistent with the asymptotic analysis.

6. Conclusions

The present work demonstrates the ability of Gao's elastic law to describe mechanical behaviour of rubber-like materials in the range of technical applications. Comparisons with Ogden's formula and Mooney–Rivlin's formula by means of a theoretical and a numerical analysis demonstrate that Gao's model performs well in describing the behaviour of hyperelastic materials and adequately covers a very large range of deformation. Discussion on Drucker's stability postulate and results of numerical calculations show that Gao's model is stable in large strain finite element analyses.

The estimation of material parameters is relatively easy since only two material parameters are used in Gao's model. The numerical simulations of three cases of simple tension are in perfect agreement with the experimental data, even when the deformation becomes very large. Furthermore, two examples prove that the material parameters estimated from simple tension tests are valid for other loading conditions if the specimens are made from the same material. This property is crucial for the general use of Gao's elastic law.

As an application, a singular problem of a wedge loaded by a concentrated tensile force is analysed based on this elastic law. The numerical results are consistent with the asymptotic analysis.

Acknowledgement

The authors wish to thank Gregory Chagnon and his colleagues for providing the experimental data.

References

Arruda, E.M., Boyce, M.C., 1993. A three-dimensional constitutive model for the large stretch behaviour of rubber elastic materials. Journal of the Mechanics and Physics of Solids 41, 389–412.

Besseling, J.A., 1983. Finite element properties, based upon elastic potential interpolation. In: Hybrid and Mixed Finite Element Methods. John Wiley & Sons, London, pp. 253–266.

van den Bogert, P.A.J., 1991. Computational modelling of rubberlike materials. PhD thesis, Delft University of Technology.

Boyce, M.C., 1996. Direct comparison of the Gent and the Arruda–Boyce constitutive models of rubber elasticity. Rubber Chemistry and Technology 69, 781–785.

Boyce, M.C., Arruda, E.M., 2000. Constitutive models of rubber elasticity: a review. Rubber Chemistry and Technology 73, 504–523.

Chagnon, G., Verron, E., Gornet, L., Marckmann, G., Charrier, P., 2004. On the relevance of continuum damage mechanics as applied to the Mullins effect in elastomers. Journal of the Mechanics and Physics of Solids 52 (7), 1627–1650.

Charlton, D.J., Yang, J., 1994. A review of methods to characterize rubber elastic behaviour for use in finite element analysis. Rubber Chemistry and Technology 67, 481–503.

Flory, P.J., Rehner Jr., J., 1943. Statistical mechanics of cross-linked polymer networks: I. Rubberlike elasticity. Journal of Chemical Physics 11, 512–520.

Gao, Y.C., 1997. Large deformation field near a crack tip in a rubber-like material. Theoretical and Applied Fracture Mechanics 26, 155–162.

Gao, Y.C., 1999. Foundation of Solid Mechanics. Railway Publisher of China, Beijing.
Gao, Y.C., Chen, H.S., 2001. Analysis of a rubber cone tensioned by a concentrated force. Mechanics Research Communications 28 (1), 49–54.
Gent, A.N., 1996. A new constitutive relation for rubber. Rubber Chemistry and Technology 69, 59–61.
Guo, Z., Sluys, L.J., Stroeven, P., Hendriks, Ch.F., 2003. Advanced computational modelling of the mechanical behaviour of rubber-like materials. In: Busfield, J.J.C., Muhr, A.H. (Eds.), Proceeding of the Third European Conference on Constitutive Models for Rubber, London. pp. 185–192.
James, H.M., Guth, E., 1941. Elastic and thermoelastic properties of rubber like materials. Industrial and Engineering Chemistry 33, 624–629.
James, H.M., Guth, E., 1943. Theory of elastic properties of rubber. Rubber Chemistry and Technology 11, 455–481.
Johnson, A.R., Quigley, G.J., Mead, J.L., 1994. Large strain viscoelastic constitutive models for rubber, part I: formulations. Rubber Chemistry and Technology 67, 904–917.
Knowles, J.K., Sternberg, E., 1973. An asymptotic finite deformation analysis of the elasto-static field near the tip of a crack. Journal of Elasticity 3, 67–107.
Kuhn, W., Grun, F., 1942. Beziehungen zwischen elastischen Konstanten und Dehnungsdoppelbrechung hochelastischer stoffe. Kolloidn Zhurnal 101, 248–271.
Miehe, C., Göktepe, S., Lulei, F., 2004. A micro-macro approach to rubber-like materials—Part I: The non-affine micro-sphere model of rubber elasticity. Journal of the Mechanics and Physics of Solids 52, 2617–2660.
Mooney, M.A., 1940. A theory of large elastic deformation. Journal of Applied Physics 11, 582–592.
Mullins, L., Tobin, N.R., 1957. Theoretical model for the elastic behaviour of filler-reinforced vulcanized rubbers. Rubber Chemistry and Technology 30, 551–571.
Ogden, R.W., 1972a. Large deformation isotropic elasticity—on the correlation of theory and experiment for the incompressible rubber-like solids. Proceedings of the Royal Society of London A 326, 565–584.
Ogden, R.W., 1972b. Large deformation isotropic elasticity—on the correlation of theory and experiment for the compressible rubber-like solids. Proceedings of the Royal Society of London A 328, 567–583.
Ogden, R.W., 1984. Non-linear elastic deformation. Dover Publications, Inc., Mineola, New York.
Ogden, R.W., 2001. Nonlinear Elasticity. Cambridge University Press, Cambridge.
Ogden, R.W., Roxburgh, D.G., 1999. A pseudo-elastic model for the Mullins effect in filled rubber. Philosophical Transactions of the Royal Society of London A 455, 2861–2877.
Pozivilova, A., 2003. Constitutive modelling of hyperelastic materials using the logarithmic description. PhD thesis, CTU Report, vol. 7, 4, Czech Technical University, Prague.
Rivlin, R.S., 1948a. Large elastic deformations of isotropic materials I. Fundamental concepts. Philosophical Transitions of the Royal Society of London A 240, 459–490.
Rivlin, R.S., 1948b. Large elastic deformations of isotropic materials IV. Further developments of the general theory. Philosophical Transitions of the Royal Society of London A 241, 379–397.
Rivlin, R.S., 1949. A note on the torsion of incompressible highly-elastic cylinder. Proceedings of the Cambridge Philosophical Society 45, 485.
Tarantola, A., 1987. Inverse Problem Theory, Methods for Data Fitting and Model Parameter Estimation. Elsevier Science Publishers B.V., The Netherlands.
Treloar, L.R.G., 1946. The elasticity of a network of long-chain molecules. Transactions of Faraday Society 42, 83–94.
Treloar, L.R.G., 1958. The Physics of Rubber Elasticity, second ed. Oxford University Press, Glasgow.
Wang, M.C., Guth, E., 1952. Statistical theory of networks of non-Gaussian flexible chains. Journal of Chemical Physics 20, 1144–1157.
Wu, P.D., van der Giessen, E., 1993. On improved network models for rubber elasticity and their applications to orientation hardening in glassy polymers. Journal of the Mechanics and Physics of Solids 41, 427–456.
Yeoh, O.H., 1993. Some forms of strain energy function for rubber. Rubber Chemistry and Technology 66, 754–771.